PHYSICAL REVIEW B VOLUME 18, NUMBER 10 15 NOVEMBER, 1978

# Determination of the self-consistent band structure of $CrCl_3$, $CrBr_3$, $NiCl_2$, and $NiBr_2$ by the intersecting-spheres model

S. Antoci and L. Mihich
*Istituto di Fisica Generale "A. Volta," Pavia, Italy*
*and Gruppo Nazionale di Struttura della Materia del Consiglio Nazionale delle Ricerche, Italy*
(Received 24 March 1978)

It has been proven previously that the intersecting-spheres model is capable of providing accurate band structures for Si and Ge. In order to compute the electronic structure of solids with a complicated unit cell, the intersecting-spheres model has been simply modified to neglect the core states in the secular equations without significant loss of accuracy. The model formulated in this way has been used to determine the self-consistent band structure of $CrCl_3$, $CrBr_3$, $NiCl_2$, and $NiBr_2$; the electronic structures of all these materials turned out to be essentially similar. For $NiCl_2$ and $NiBr_2$, our results were compared with existing photoemission data, and satisfactory agreement between calculated and observed structures was found. For all the crystals investigated, a comparison was also made with ultraviolet optical and thermoreflectance data; through this comparison it seems possible to attempt a unique interpretation of the observed spectra in terms of transitions occurring between the occupied halogen $p$ bands and the unoccupied metal $s$ and $p$ bands.

## I. INTRODUCTION

In a recent paper it has been shown that the computation of the electronic structure of Si and Ge performed by the intersecting-spheres model[1] gives results in good agreement with orthogonalized-plane-wave calculations performed under the same assumptions for the self-consistent potential.

Further test calculations[2] of the electronic structure of quite different crystals like $(SN)_x$, Al, and TiO indicate that the model is of rather general applicability. In order to afford the determination of the electronic structure of solids with a complicated unit cell and rather heavy constituent atoms it may be useful to neglect the core states in the calculations. This modification can be easily introduced; in fact the intersecting-spheres model adopts trial functions for the core states and for the valence states which are very nearly mutually orthogonal. This near orthogonality is ensured by the peculiar form of the warped atomiclike orbitals[1]: the core states of a given atom are automatically orthogonal to the unwarped valence orbitals of the same atom since all these functions are generated by the solution of an eigenvalue problem with the same boundary conditions; the subsequent warping, while not destroying the orthogonality in a relevant way, does not allow any significant overlap of the warped valence orbitals centered on neighboring atoms with the above-mentioned core states. Due to this near orthogonality not only the overlap matrix elements but also the Hamiltonian matrix elements between core and valence warped orbitals should be negligible. In fact the unwarped functions are solutions of the self-consistent atomic problem and therefore the above-mentioned Hamiltonian matrix elements calculated with the atomic potential are nearly zero. Since the correction to the potential in the core regions due to the crystalline environment predominantly consists of a constant term we expect that the above-mentioned matrix elements calculated with the actual crystal potential should be negligible.

If this expectation is realized in practice we can simply drop the core states from the secular equations of the intersecting-spheres model without further adjustment. For what concerns the self-consistent potential it is then possible to introduce the frozen-core approximation. We have verified[2] that the scheme outlined above works well in practice since the neglect of the core states in the secular equations calculated with the atomic potential alters the valence eigenvalues at most $10^{-4}$ eV, while self-consistent band energies obtained with an all-electron calculation and with the above-mentioned approximations typically differ by 0.02 eV in the valence region. With the modification outlined above the intersecting-spheres model is well suited to the computation of the band structure of solids with a complicated unit cell.

In this article we report on the self-consistent calculation of the electronic structure of $CrCl_3$, $CrBr_3$, $NiCl_2$, and $NiBr_2$ and we compare the results with existing photoemission and ultraviolet optical data.

## II. $CrCl_3$ AND $CrBr_3$ BAND STRUCTURE

The low-temperature structure of the layer crystals $CrCl_3$ and $CrBr_3$ is reported in Ref. 3. The three-dimensional unit cell of these crystals is rombohedral and contains two chromium and six halogen atoms.

The length $a$ of the primitive translation vector

 

for $CrCl_3$ and $CrBr_3$ was assumed to be 12.668 and 13.346 a.u., respectively, as inferred from Ref. 4. The primitive vectors and the coordinates of chromium and halogen atoms in the unit cell are reported in Table I(a). It can be recognized that the six halogen atoms nearest neighbors to each chromium atom are arranged on a regular octahedron.

The isogonal point group of the space group of these crystals is $C_{3i}$ and the classification of the levels at the various points and lines of symmetry of the Brillouin zone, shown in Fig. 1, has been performed accordingly (see also Ref. 5). The coordinates of the symmetry points contained in the irreducible segment of the Brillouin zone are reported in Table II(a).

As required by the intersecting-spheres model we surrounded all the atoms of the crystal with spheres, we inserted cylindrical regions between neighboring sphers and we derived a cellular partition into atomic cells and spline regions in the manner indicated in Ref. 1. Assuming a local exchange correlation potential of the Kohn-Sham type we than solved the self-consistent Schrödinger equation within each atomic sphere, thus generating atomiclike orbitals which were warped according to the prescriptions described in Ref. 1. We have then built Bloch sums using the 4*s*, 5*s*, 6*s*, 4*p*, 5*p*, 3*d*, 4*d* warped atomic orbitals for Cr, the 3*s*, 4*s*, 5*s*, 3*p*, 4*p*, 3*d* orbitals for Cl and the 4*s*, 5*s*, 6*s*, 4*p*, 5*p*, 4*d* orbitals for Br, respectively.

With this choice for the valence functions and with the spatial partition adopted by us the requirement of orthogonality of the valence Bloch sums to the core states is very nearly fulfilled; the above-mentioned choice also allows satisfactory flexibility of the overall trial function. In fact, with such a choice the energy levels associated with the valence and the lower conduction bands of

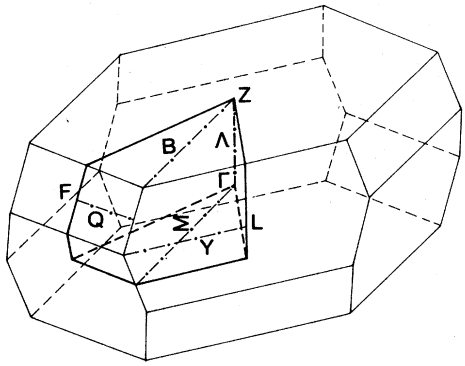


FIG. 1. Sketch of the Brillouin zone occurring for $CrCl_3$, $CrBr_3$ and also for $NiCl_2$, $NiBr_2$. Γ, *Z*, *L*, *F* are the symmetry points reported in Table II, while Σ, Λ, *Y*, *Q*, and *B* are symmetry lines (dash dotted). The irreducible segment is also drawn.

TABLE I. (a) Unit vectors and position vectors of the atoms in the unit cell of $CrCl_3$ and $CrBr_3$ (*a* units). *h* stands for halogen. (b) Unit vectors and position vectors of the atoms in the unit cell of $NiCl_2$ and $NiBr_2$ (*a* units). *h* stands for halogen.

(a)

| | *x* | *y* | *z* |
|---|---|---|---|
| $\tau_1$ | 0 | −0.5118 | 0.8591 |
| $\tau_2$ | 0.4432 | 0.2559 | 0.8591 |
| $\tau_3$ | −0.4432 | 0.2559 | 0.8591 |
| $Cr_{(1)}$ | 0 | 0 | 0.4295 |
| $Cr_{(2)}$ | 0 | 0 | −0.4295 |
| $h_1$ | 0.1477 | −0.2559 | 0.2206 |
| $h_2$ | 0.1477 | 0.2559 | 0.2206 |
| $h_3$ | −0.2955 | 0 | 0.2206 |
| $h_4$ | −0.1477 | −0.2559 | −0.2206 |
| $h_5$ | 0.2955 | 0 | −0.2206 |
| $h_6$ | −0.1477 | 0.2559 | −0.2206 |

(b)

| | *x* | *y* | *z* |
|---|---|---|---|
| $\tau_1$ | 0 | $-\frac{1}{3}$ | $2\sqrt{2}/3$ |
| $\tau_2$ | $\sqrt{3}/6$ | $\frac{1}{6}$ | $2\sqrt{2}/3$ |
| $\tau_3$ | $-\sqrt{3}/6$ | $\frac{1}{6}$ | $2\sqrt{2}/3$ |
| Ni | 0 | 0 | 0 |
| $h_1$ | 0 | 0 | $\sqrt{2}/2$ |
| $h_2$ | 0 | 0 | $-\sqrt{2}/2$ |

TABLE II. (a) Coordinates of the symmetry points in the irreducible segment of the Brillouin zone for $CrCl_3$ and $CrBr_3$. The coordinates are given in $2\pi/a$ units. (b) Coordinates and weights of the symmetry points in the irreducible segment of the Brillouin zone for $NiCl_2$ and $NiBr_2$. The coordinates are given in $2\pi/a$ units.

(a)

| Point | $K_x$ | $K_y$ | $K_z$ |
|---|---|---|---|
| Γ | 0 | 0 | 0 |
| *Z* | 0 | 0 | 0.5820 |
| *L* | 0.5640 | 0.3256 | 0.1940 |
| *F* | 0.5640 | −0.3256 | 0.3880 |

(b)

| Point | $K_x$ | $K_y$ | $K_z$ | Weight |
|---|---|---|---|---|
| Γ | 0 | 0 | 0 | 1 |
| *Z* | 0 | 0 | $3\sqrt{2}/8$ | 1 |
| *L* | $\sqrt{3}/2$ | $\frac{1}{2}$ | $\sqrt{2}/8$ | 3 |
| *F* | $\sqrt{3}/2$ | $-\frac{1}{2}$ | $2\sqrt{2}/8$ | 3 |

$CrCl_3$ and $CrBr_3$ are rather insensitive to variations of the radii of the spheres and of the thickness of the spline regions around their optimum values, which resulted to be $R_{Cr} = R_{Cl} = 5.5$ a.u., $h_{Cr\text{-}Cl} = h_{Cl\text{-}Cl} = 0.8$ a.u. for $CrCl_3$ and $R_{Cr} = R_{Br} = 5.89$ a.u., $h_{Cr\text{-}Br} = h_{Br\text{-}Br} = 0.8$ a.u. for $CrBr_3$, respectively. The optimum values were determined as those for which the valence levels at the first cycle of the self-consistent iteration were as low as possible.

The expansion of the self-consistent potential in spherical harmonics around the various atomic centers was limited to include $l = 2$ terms after having verified that the inclusion of higher terms up to $l = 4$ did not significantly modify the band structure. Electrostatic contributions to the self-consistent potential in each atomic cell due to the neighboring cells were accounted for through spherical harmonic reexpansion[1] including up to three and four shells of neighbors for the Cr and the halogen site, respectively, while the remaining contribution was included through Madelung sums. For the exchange potential the Kohn-Sham approximation ($\alpha = \frac{2}{3}$) was assumed everywhere in the crystal. We have observed that when the full Slater exchange ($\alpha = 1$) is used the relative positions of the bands are not significantly modified with respect to the Kohn-Sham result. More significant changes occur when different values of $\alpha$ are adopted for different atomic cells. We have not attempted to empirically adjust the values of $\alpha$ for each cell since this procedure is in contrast with the *ab initio* character of these calculations: we prefer to provide results which are not dependent on the peculiarities of a model and therefore directly comparable with results obtained with other methods adopting different or no cellular partitions.

For what concerns the sum over the Brillouin zone used to calculate the self-consistent charge density, it was limited to a single $\vec{K}$ point ($\Gamma$). This choice was primarily motivated by the big computational effort required by the self-consistent procedure, but it resulted *a posteriori* to allow satisfactory accuracy, since the occupied valence bands of $CrCl_3$ and $CrBr_3$ fortunately display very small dispersion.

In Figs. 2 and 3 we present the self-consistent band structure of $CrCl_3$ and $CrBr_3$ along a contour including the symmetry lines. Figures 2 and 3 do not display the lower-lying valence bands associated with Cl 3*s* and Br 4*s* atomic levels, which were comprised in the calculations. They range between −17.2 and −15.8 eV for $CrCl_3$ and lie between −16.5 and −15.0 eV for $CrBr_3$.

We can observe that the band structures of $CrCl_3$ and of $CrBr_3$ are very similar. Going upward along the energy scale we first encounter eighteen valence bands covering an energy interval of 4.6 eV in $CrCl_3$ and of 4.9 eV in $CrBr_3$, respectively.

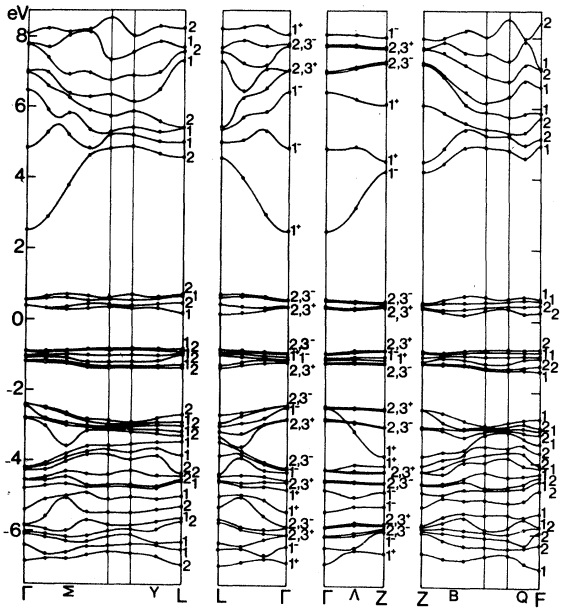


FIG. 2. Self-consistent band structure of $CrCl_3$ along a contour connecting and including the symmetry lines shown in Fig. 1.

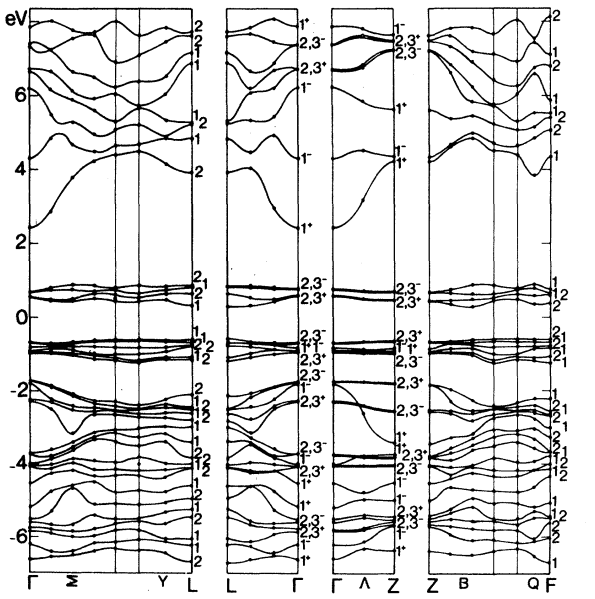


FIG. 3. Self-consistent band structure of $CrBr_3$ along a contour connecting and including the symmetry lines shown in Fig. 1.

The dispersion of the individual bands is not larger than 1.6 eV along each symmetry line. The investigation of the eigenvectors shows that these bands have predominantly Cl $3p$ or Br $4p$ character. We find then two groups of six and four bands with very small dispersion (at most 0.3 eV). These levels turn out to be essentially associated with Cr $3d$ atomic orbitals. Since the crystal potential around each Cr site has approximate octahedral symmetry it is reasonable that the bands are clustered in two groups of six and four levels, approximately corresponding to the $T_{2g}$ and $E_g$ representations of the $O_h$ point group (we have two Cr atoms per unit cell). We note that the Fermi level lies within the lower group of bands and that in our spin restricted treatment only the equivalent of three full bands of the lower group is occupied. Above the $d$ bands we find a conduction band of Cr $4s$ character with a minimum at $\Gamma$ ($\Gamma_1^+$). Next in energy we find at $\Gamma$ a $\Gamma_1^-$ level associated with Cr $4p$ orbitals and another $\Gamma_1^-$ level predominantly constituted by Cr $4s$ orbitals. From these levels origin two bands of mixed $s$-$p$ character, while the remaining four bands shown in Figures 2 and 3 have predominantly Cr $4p$ character.

## III. $NiCl_2$ AND $NiBr_2$ BAND STRUCTURE

The crystal structure of $NiCl_2$ and of $NiBr_2$ is reported in Ref. 6. The Bravais lattice can be assumed to be trigonal primitive and the rombohedral unit cell contains now one Ni and two halogen atoms. The length $a$ of the primitive translation vectors for $NiCl_2$ and $NiBr_2$ was assumed to be 11.584 and 12.217 a.u., respectively.[6] The primitive vectors and the coordinates of the Ni and of the halogen atoms in the unit cell are reported in Table I(b). Also in this case it can be seen that the halogen atoms are arranged on regular octahedra surrounding each Ni atom. The isogonal point group of the space group for these crystals is now $D_{3d}$. The three-dimensional Brillouin zone is again shown in Fig. 1. The coordinates of the symmetry points and their weight for integration over the Brillouin zone are reported in Table II(b).

The spatial partition needed by the intersecting-spheres model was performed as indicated previously for $CrCl_3$ and $CrBr_3$. We assumed again a local exchange correlation potential of the Kohn-Sham type and we generated the basis set as previously shown. Bloch sums were built in this case using for the metal and for the halogens the same choice of atomiclike orbitals as that adopted for $CrCl_3$ and $CrBr_3$. The radii of the spheres and the thickness of the cylinders turned out to be $R_{Ni} = R_{Cl} = 5.6$ a.u., $h_{Ni\text{-}Cl} = h_{Cl\text{-}Cl} = 0.8$ a.u. for $NiCl_2$ and $R_{Ni} = R_{Br} = 5.9$ a.u., $h_{Ni\text{-}Br} = h_{Br\text{-}Br} = 0.8$ a.u. for $NiBr_2$, respectively. The expansion of the self-consistent potential in spherical harmonics was truncated at $l = 4$ with very satisfactory convergence. Contributions to the potential in an atomic cell due to the other cells were treated through spherical harmonics reexpansion up to four shells of neighbors and the remaining terms were treated through Madelung sums. Since for $NiCl_2$ and $NiBr_2$ the self-consistent calculations require a rather small numerical effort we have been able to compute the self-consistent charge density by substituting the integral over the Brillouin zone with a weighted sum over the four points indicated in Table II(b).

We have verified by performing the same calculations with a single point ($\Gamma$) in the sum that the convergence is indeed satisfactory, since we did not find changes in the relative position of the valence levels greater than 0.2 eV when the two above mentioned calculations were compared. This result supports also the validity of the single point sampling adopted for $CrCl_3$ and $CrBr_3$: the dispersion of the valence bands in that case is in fact smaller than in the case of $NiCl_2$ and $NiBr_2$.

In Figs. 4 and 5 the self-consistent band structures of $NiCl_2$ and $NiBr_2$ are reported (the low-ly-

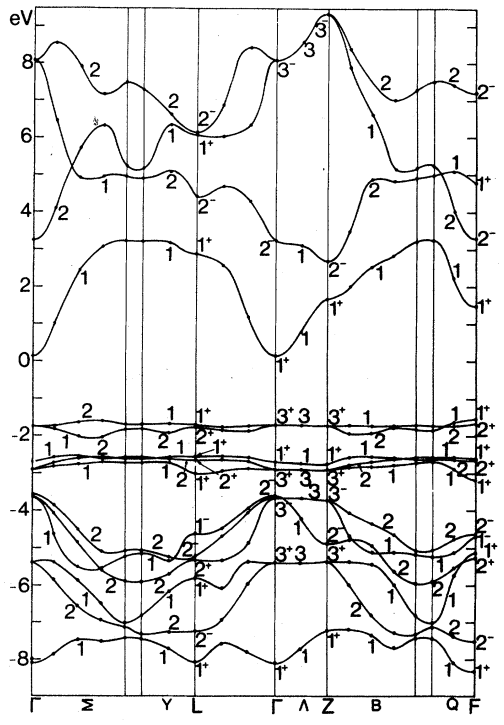


FIG. 4. Self-consistent band structure of $NiCl_2$ along a contour connecting and including the symmetry lines shown in Fig. 1.

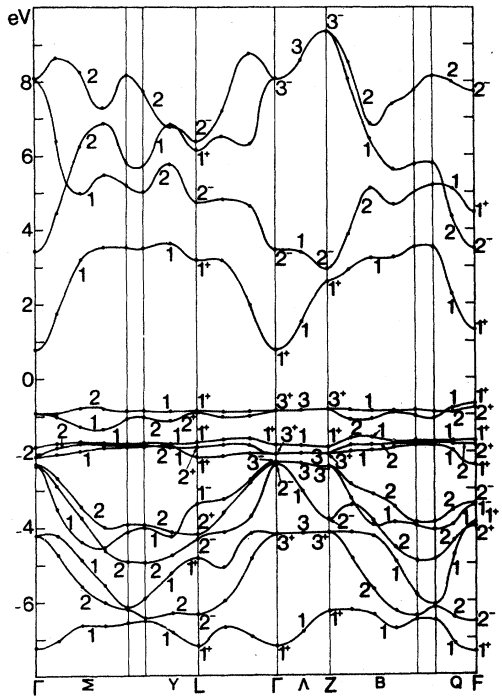


FIG. 5. Self-consistent band structure of $NiBr_2$ along a contour connecting and including the symmetry lines shown in Fig. 1.

ing bands associated with Cl 3*s* or Br 4*s* atomic levels are not shown in Figures 4 and 5; they fall between −18.0 and −16.8 eV for $NiCl_2$, and lie between −16.6 and −15.4 eV for $NiBr_2$, respectively).

In Figs. 4 and 5 we note six valence bands of essentially halogen 3*p* or 4*p* character covering an energy interval of 4.5 and 5.0 eV for $NiCl_2$ and $NiBr_2$, respectively. These bands correspond to the eighteen *p* valence bands found in the case of $CrCl_3$ and $CrBr_3$. We find then five Ni *d* bands divided in two groups of three and two as must be expected from the near octahedral symmetry of the Ni site. These bands display very small dispersion; the Fermi level falls now within the upper doublet, which has a population equivalent to one fully occupied band. Above these *d* levels we find an isolated conduction band predominantly of Ni 4*s* character with a dispersion of about 3 eV and three more bands of Ni 4*p* character. Concluding this description of the results we note that, despite the differences in the crystal structure, the electronic structures of $NiCl_2$ and $NiBr_2$ are qualitatively very similar to those of $CrCl_3$ and $CrBr_3$.

## IV. COMPARISON WITH PHOTOEMISSION DATA

If the valence-band structure of $NiCl_2$ and $NiBr_2$ calculated by us is directly utilized to predict the photoemission spectra we should expect in the high-energy side a doublet structure associated with the Ni *d* bands, with a separation of about 0.8 eV for both crystals; measuring the binding energies from the top levels of the doublet we should expect structures associated with the halogen *p* bands ranging from −1.8 to −6.6 eV for $NiCl_2$ and lying between −1.3 and −6.4 eV for $NiBr_2$. We should then find a rather sharp structure associated with the narrow halogen *s* bands occurring at −15.7 eV for $NiCl_2$ and at −15.0 eV for $NiBr_2$. Experimental photoemission data for $NiCl_2$ and for $NiBr_2$ are reported in the literature.[7,8] Since we have performed only a spin restricted calculation for the ground state within a one-electron formalism we cannot expect to find precise agreement with experimental data in particular for the *d* levels. Many-body effects influencing the photoemission spectra are neglected in the band description; we therefore caution the reader not to take possible agreement between the results of these calculation and the experimental data as really conclusive. It is however surprising to note that when we compare our results for $NiCl_2$ with the well resolved spectrum of Ref. 7, shown in Fig. 6, our predictions are fulfilled with rather good accuracy. In particular the separation between the high-

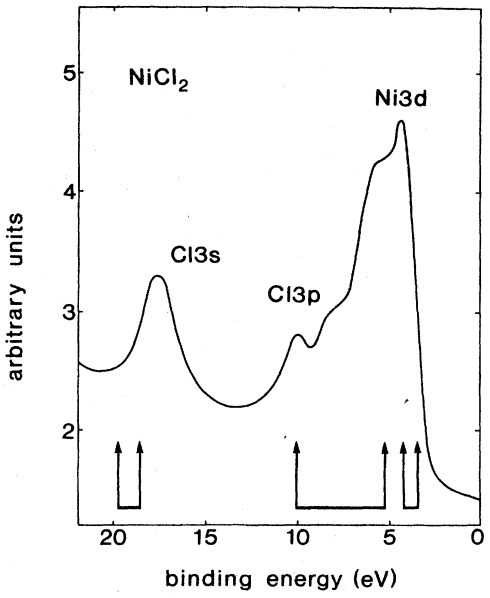


FIG. 6. X-ray photoemission valence-band spectrum of $NiCl_2$ according to Ref. 7. The peak assignments of Ref. 7 are also reported. The arrows mark, from right to left, the upper and lower limits of the Ni 3*d*, Cl 3*p*, and Cl 3*s* bands, respectively, as resulting from the present calculations. The band structure has been shifted rigidly to put the highest occupied *d* band in coincidence with the onset of the photoemission spectrum.

energy onset of the photoemission spectrum and the isolated peak marking the position of the $s$ levels is 14 eV according to Ref. 7 and 15–16 eV in Ref. 8. Furthermore, the separation of the middle peak seen in Ref. 7 and presumably marking the bottom of the $p$ valence band from the above mentioned onset is about 7 eV.

In Ref. 8 broad structures are reported for both $NiCl_2$ and $NiBr_2$ (apart from the $s$ peaks) and are entirely attributed to $d$ levels spread in an energy interval much larger than predicted by us. It is claimed that such an interpretation is necessary to explain the observed similarity of the photoemission spectra of $NiCl_2$ and $NiBr_2$; it is argued that, if the spectra were due also to $p$ contributions, they should appear quite different, since the $p$ bands of Cl should be different from those of Br. Our calculations however indicate that $NiCl_2$ and $NiBr_2$ have a very similar structure of the valence $p$ bands; therefore the arguments of Ref. 8 seem not to be valid. We believe that the interpretation of the photoemission spectrum of $NiCl_2$ reported in Ref. 7 is correct and that is should apply also to $NiBr_2$. To our knowledge the photoemission spectra of $CrCl_3$ and $CrBr_3$ are not present in the literature; according to our calculated band structures they should look very similar to the spectra of the Ni halides (except for the $d$ region).

## V. COMPARISON WITH OPTICAL DATA

For what concerns optical measurements much information is present in the literature for all the crystals investigated by us.[9-12]

The low-energy part of the spectra is dominated by weak $d \rightarrow d$ transitions[9] and its interpretation is evidently beyond the possibilities of a calculation with a one-electron formalism. For the same reasons we cannot safely predict charge transfer and orbital promotion transitions beyond a generic information concerning their energy range. We can however hope to predict with some more affidability where the interband gaps between the valence $p$ bands and the conduction $s$ and $p$ bands occur in the spectra. In view of the low dielectric constant of these materials we should expect that the exciton interaction may give rise to marked structures associated with interband gaps. We therefore attempt to correlate the sharp structures observed by reflectance and thermoreflectance measurements on single crystals[11,12] with the calculated interband gaps. Since the above mentioned measurements were performed with light incident normally to the layer planes only transitions allowed for this configuration need to be considered at present.

In the case of $CrCl_3$ and $CrBr_3$ the first allowed interband transition is predicted to occur at $\Gamma$ between the top of the $p$ valence band ($\Gamma_2^-$, $\Gamma_3^-$) and the bottom of the $s$ conduction band ($\Gamma_1^+$) at 4.9 and 4.2 eV, respectively. It seems reasonable to associate this gap with the strong peak observed in thermoreflectance at 4.3 eV in $CrCl_3$ and with the strong doublet (a spin-orbit doublet?) centered at about 3.8 eV in $CrBr_3$. The strength of these structures, clearly shown in Fig. 7, where the imaginary part of the experimental dielectric function $\epsilon_2$ is reported, seems to indicate that a true interband transition rather than a charge transfer transition is involved. Orbital promotion to the $s$ level is discarded by symmetry arguments. According to the calculated band structures and apart from possible saddle points we do not expect other strong interband transitions to occur up to 7.5 eV in $CrCl_3$ and up to 6.5 eV in $CrBr_3$; at these energies we find allowed gaps between the highest $\Gamma_2^+$ and $\Gamma_3^+$ valence levels and the lowest $\Gamma_1^-$ conduction level. From these energies on we find many contributions deriving from the $p$ conduction bands which should lead to an appreciable increase of the imaginary part of the dielectric function $\epsilon_2$ and to additional excitonic structure. From the experimental point of view such an increase occurs in $CrCl_3$ starting from 8 eV and in $CrBr_3$ starting from 7.3 eV. In $CrBr_3$ we find also a sharp thermoreflectance structure at 7.3 eV. We believe that the correlation found between the experimental structures and the interband gaps is something more than a pure coincidence: corresponding experimental structures are found

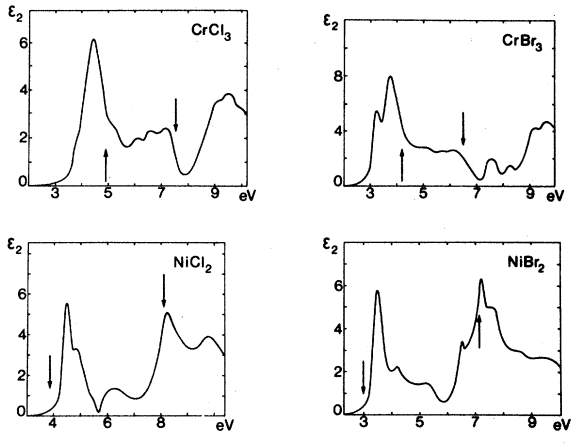


FIG. 7. Imaginary part of the dielectric function $\epsilon_2$ at $T = 80\,^{\circ}K$ for $CrCl_3$, $CrBr_3$, $NiCl_2$, and $NiBr_2$ according to Ref. 12. The arrows mark the calculated interband gaps corresponding to the onset of allowed transitions between the halogen $p$ bands and the metal $s$ and $p$ bands.

in $CrBr_3$ at lower energy than in $CrCl_3$ by about 0.7 eV and the calculated gaps closely follow this trend.

In the case of $NiCl_2$ and of $NiBr_2$ we predict that the first interband gap occurs between the top valence level $\Gamma_3^-$ and the $\Gamma_1^+$ conduction level. This gap has a width of 3.8 eV in $NiCl_2$ and of 3.0 eV in $NiBr_2$. The first strong reflectivity peak occurs at 4.4 eV in $NiCl_2$ and at 3.5 eV in $NiBr_2$ and can reasonably be associated to the first interband gap (see also the $\epsilon_2$ spectra of Fig. 7 for comparison). According to the calculated band structure and apart from possible saddle points the next allowed interband transition occurs at $Z$ between the $Z_3^+$ valence level and the $Z_2^-$ $p$ conduction level. This gap has a width of 8.1 eV in $NiCl_2$ and of 7.1 eV in $NiBr_2$. From these energies on we expect that transitions to the $p$ levels should maintain the imaginary part of the dielectric function $\epsilon_2$ to a high level. Experimentally we note that $\epsilon_2$ displays a sharp rise at about 8 eV in $NiCl_2$ and at about 6.5 eV in $NiBr_2$. This rise in accompanied by sharp structures seen in thermoreflectance at 8.5 eV in $NiCl_2$ and at 7.2 eV in $NiBr_2$ (the additional sharp structure at 6.6 eV which tends to disappear at low temperature is presently a puzzle). We note that also for the Ni halides corresponding structures shift to lower energy about 1 eV when Cl is replaced by Br and that such a behavior is replicated by the theoretical gaps.

## VI. CONCLUSIONS

For $NiCl_2$ (and $NiBr_2$) the calculations reported in this article support one of the two interpretations of the photoemission spectra reported in the literature. For all the crystals investigated they suggest an unique interpretation for the main structures of the ultraviolet optical spectra. According to this interpretation the peaks occurring in the low-energy side of the ultraviolet spectra should originate from gaps between the halogen $p$ levels and the metal $s$ levels, while the structures in the high-energy side of the spectra should derive from transitions between the halogen $p$ levels and the metal $p$ levels.

## ACKNOWLEDGMENTS

We are indebted to Professor E. Clementi for stimulating this research and for providing the means for its accomplishment. We thank also Dr. L. Nosenzo and Professor G. Samoggia for illustrating the experimental results. This research was supported by the Instituto di Ricerche "G. Donegani," Novara, Italy.

[1]S. Antoci and L. Mihich, Phys. Rev. B 17, 1859 (1978).
[2]S. Antoci and L. Mihich (unpublished).
[3]I. Tsubokawa, J. Phys. Soc. Jpn. 15, 1664 (1960).
[4]J. F. Dillon Jr., H. Kamimura, and J. P. Remeika, J. Phys. Chem. Solids 27, 1531 (1966).
[5]C. J. Bradley and A. P. Cracknell, *The Mathematical Theory of Symmetry in Solids* (Clarendon, Oxford, 1972).
[6]R. W. G. Wyckoff, *Crystal Structure* (Interscience, New York, 1964).
[7]S. Hufner and G. K. Wertheim, Phys. Rev. B 8, 4857 (1973).
[8]Y. Sakisaka, T Ishii, and T. Sagawa, J. Phys. Soc. Jpn. 36, 1372 (1974).
[9]See, for example, D. L. Wood, J. Ferguson, K. Knox, and J. F. Dillon Jr., J. Chem. Phys. 39, 890 (1963).
[10]Y. Sakisaka, T. Ishii, and T. Sagawa, J. Phys. Soc. Jpn. 36, 1365 (1974).
[11]I. Pollini and G. Spinolo, J. Phys. C 7, 2391 (1974).
[12]G. Guizzetti, L. Nosenzo, I. Pollini, E. Reguzzoni, G. Samoggia, and G. Spinolo, Phys. Rev. B 14, 4622 (1976).